Boiling Heat Transfer Coefficient and Critical Heat Flux on Conical Cylindrical Copper under Surface Modification

Muhammad Dimyati Nashrullah[1*], Andi Sanata[1], Imam Solahuddin[1], Nasrul Ilminnafik[1], Indro Pranoto[2], Adhika Widyaparaga[2]

[1]*Department of Mechanical Engineering, University of Jember, Sumbersari, Jember, 68121, Indonesia*
[2]*Department of Mechanical and Industrial Engineering, Universitas Gadjah Mada, Mlati, Sleman, 55281, Indonesia*
**Corresponding author: m.dimyati.nashrullah@unej.ac.id*

Article history:
Received: 28 December 2024 / Received in revised form: 27 March 2025 / Accepted: 17 April 2025
Available online 6 May 2025

ABSTRACT

This study examined how surface roughness and nanoceramic coating, influences the boiling heat transfer coefficient (BHTC) and critical heat flux (CHF) of a conical cylindrical copper test specimen. Three test specimens exhibiting surface roughness of 0.22 µm, 0.14 µm, and 0.04 µm were analyzed for comparison. Two additional test specimens were treated with nanoceramic coatings utilizing silicon carbide as the base material: one specimen received a single-layer coating and the second was applied with a double-layer coating. The behavior of the bubbles was closely observed with a high-speed camera to deepen the analysis. The experimental results showed that the test specimen with higher surface roughness exhibited higher BHTC and CHF. The 0.22 µm surface roughness specimen demonstrated a 55.69% greater BHTC than the 0.04 µm surface roughness specimen. In contrast, the 0.04 µm surface roughness specimen had the lowest CHF, 426.09 kW/m². Nanoceramic coating also enhanced the BHTC and CHF. The specimen with a single-layer coating had the highest BHTC, 40.81% higher than the uncoated specimen. The specimen with a double-layer coating showed a 60.12% increase in CHF compared to the specimen with a single-layer coating. The bubble observation results indicated that test specimens with higher BHTC and CHF had more active nucleation sites. The quantity of active nucleation sites plays a vital role in producing a large number of bubbles, enhancing heat transfer, and maintaining the surface temperature.

Keywords: *Boiling heat transfer coefficient, critical heat flux, nanoceramic coating, surface roughness.*

I. Introduction

High heat flux devices find extensive applications across various industries, including fuel cells, microprocessors, nuclear power plants, radar systems, aerospace, and defense sectors [1]-[4]. Cooling systems capable of transferring high heat flux are increasingly required to ensure the continuous operation of such devices. Many cooling methods have been developed, such as natural convection cooling, single-phase cooling, immersion cooling, spray cooling, and jet impingement cooling. Among these methods, it is known that pool boiling has superior cooling potential compared to other cooling techniques [5]. Pool boiling also has other advantages, such as simplicity and passive operation. A comparison of the cooling potential of pool boiling with other cooling methods is shown in Figure 1.

Several techniques have been applied to enhance the heat transfer performance in pool boiling. Research results indicate that surface structure significantly affects pool boiling performance [7]. Surface modification involves altering the surface structure, including adjusting surface roughness, changing the geometry of the heating surface, utilizing porous

DOI: 10.17977/um016v9i12025p126

structures, and applying micro and nanoparticle coatings to the heating surface [2],[8]-[13]. Another method employed to improve pool boiling performance involves the utilization of various working fluids, the implementation of nanofluids, and additional approaches, including the application of magnetic fields and vibrations [14]-[19]. Other experimental conditions, such as the effects of microgravity, high pressure, and low pressure on pool boiling, were also observed [20]-[22].

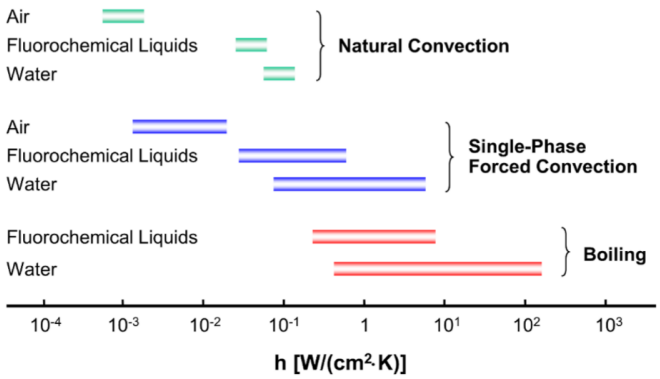

Fig. 1. Comparison of cooling methods [6]

Nukiyama conducted the first pool boiling experiment [23]. Based on Nukiyama's curve, pool boiling is divided into regimes: natural convection boiling, nucleate boiling, transition boiling, and film boiling. Among these four regimes, the nucleate boiling regime exhibits the highest transfer performance while keeping the surface temperature at a relatively low level. The nucleate boiling regime's heat transfer capability arises from the continuous formation of bubbles that transport heat away from the surface [24]. Many studies have been conducted to improve boiling heat transfer performance, specifically increasing the boiling heat transfer coefficient (BHTC) within the nucleate boiling regime. Researchers have also focused on improving the upper limit of the BHTC, which occurs at the critical heat flux (CHF) [25]. Figure 2 illustrates the optimal approach for improving pool boiling performance.

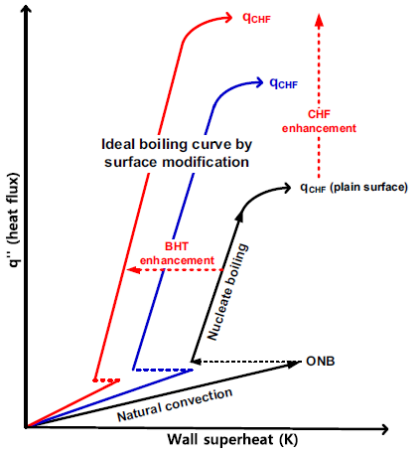

Fig. 2. Ideal scheme of a pool boiling curve [29]

Cooling processes using the pool boiling phenomenon are undesirable when approaching the CHF point within the nucleate boiling regime. The BHTC decreases after the CHF point, even as the surface temperature increases. Moreover, if heat transfer

continues beyond the CHF point or through the nucleate boiling regime, it can lead to dangerous phenomenon such as dry-out and burnout in the system being cooled [26],[27]. Therefore, improving heat transfer performance within the nucleate boiling regime represents the most effective and secure method for advancing heat transfer in pool boiling..

The CHF is the maximum amount of heat that a fluid may transport in pool boiling, whereas the BHTC is a coefficient that affects how much heat the fluid transfers. Increasing the BHTC in a pool boiling cooling system can reduce the required size, volume, and energy. Meanwhile, enhancing the CHF allows the system to be more compact and operate at higher heat fluxes. A cooling system with a low CHF is very dangerous because it has a dry-out point at a lower temperature. If this dry-out phenomenon occurs during the cooling process, the heat flux transfer will not operate effectively [28].

The high potential of pool boiling for heat transfer has not yet been accompanied by universally accepted physical mechanisms and theoretical predictions. This is primarily due to the intensity and complexity of bubble dynamics inherent in the pool boiling phenomenon [30],[31]. Pool boiling studies often focus on the behavior of bubbles as heat carriers. Bubble observation is conducted by examining the dynamics of a single bubble as well as the interactions between bubbles [32]. In addition, the performance parameters in pool boiling are also influenced by surface wettability, pore structure formation, liquid spreadability, capillarity and wickability, porosity, critical pressure, and Rayleigh-Taylor instability wavelength [33].

Although surface roughness and nanoceramic coatings have been shown to influence heat transfer performance in pool boiling phenomenon, the physical mechanisms underlying this enhancement are not yet fully understood. How surface roughness and the nanostructure of the coating on the surface affect the formation and release of vapor bubbles and how surface roughness and nanoceramic coatings influence active nucleation sites and bubble dynamics still require further exploration. Additionally, while many studies focus on improving the BHTC, research on how surface roughness and nanoceramic coatings impact the CHF point remains underexplored. Yet, CHF is a critical parameter that determines the safe operational limits of cooling systems. A deeper understanding of the physical mechanisms behind the enhancement of BHTC and CHF through the combination of surface roughness and nanoceramic coatings could aid in designing more efficient and safer cooling systems.

This study further investigates the impact of surface modification on the pool boiling phenomenon, specifically within the nucleate boiling regime. Experiments on pool boiling will be conducted at atmospheric pressure and saturation temperature utilizing deionized water as the working fluid. Five test specimens are made of copper in a conical cylindrical shape, with three variations of surface roughness and three with nanoceramic coating applications. To comprehend the pool boiling phenomenon, a high-speed camera will be used to examine how surface alteration affects BHTC, CHF, and bubble behavior.

II. Material and Methods

1. Test Specimens

This study involved the preparation of five test specimens made from copper, designed in a conical cylindrical shape. These specimens had a thermal conductivity of 382 W/m·K and featured a surface cross-section diameter of 30 mm. Figure 3 illustrates the dimensions of the test specimens (in mm). Each test specimen features three holes, each with a diameter

of 1.2 mm, designed for the placement of K-type thermocouples to accurately measure the surface temperature. Furthermore, four holes measuring 6 mm in diameter and 50 mm in depth have been designated for the installation of the cartridge heaters.

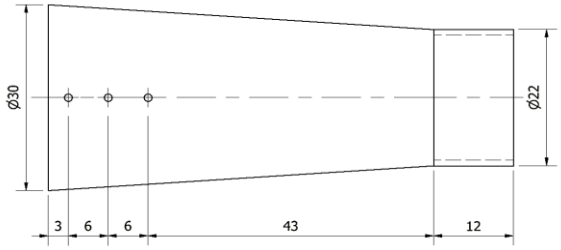

Fig. 3. Test specimens dimensions

Three test specimens were subjected to surface roughness modification, and two test specimens were coated with nanoceramics. The surface roughness variations of the test specimens were obtained by polishing the surfaces using sandpaper and Autosol. The surface of specimen A underwent polishing with 600-grit sandpaper. The surface of specimen B underwent polishing with 600, 1000, and 2000-grit sandpapers sequentially. The surface of specimen C underwent a polishing process utilizing 600, 1000, 2000, and 5000-grit sandpapers, followed by the application of Autosol in a sequential manner. The surface modification's roughness results were measured utilizing a Stillo profilometer.

The test specimens subjected to surface roughness modifications, which resulted in the roughness values, are shown in Table 1. The cross-sectional results of the surface roughness modification and the contact angle results for test specimens A, B, and C can be seen in Figure 4 and 5, respectively. For the test specimens with nanoceramic coating, specimens C-1 and C-2 were first subjected to the same surface roughness treatment as specimen C. Then, specimens C-1 and C-2 were coated with Bodyguard S36 nanoceramic coating from TEVO Creation Inc., which has a silicon carbide base material with a thermal conductivity of 20.7 W/m·K. The coating application involved a single layer for specimen C-1, while specimen C-2 received two layers. This experiment was conducted within a limited range of surface roughness values, coating thicknesses, and types of nanoceramic coatings. Different parameters of surface roughness and nanoceramic coatings may yield different results.

Table 1. Surface roughness treatment

Test specimens	Surface roughness treatment	R_a (µm)	R_{max} (µm)	R_z (µm)
A	Polished using 600-grit sandpaper	0.22	2.74	2.1
B	Polished using 2000-grit sandpaper	0.14	1.48	1.18
C	Polished using 5000-grit sandpaper and Autosol	0.04	0.32	0.26

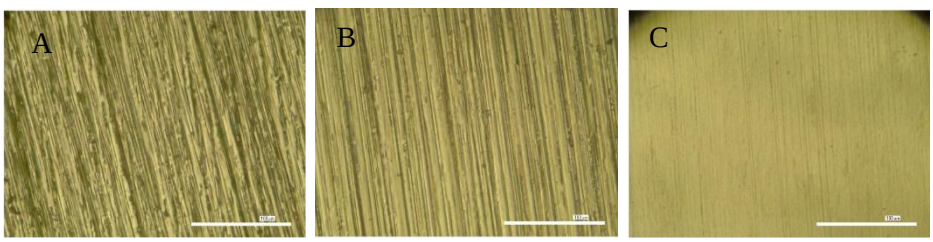

Fig. 4. Surface visualization of the test specimen at 100x magnification under the microscope.

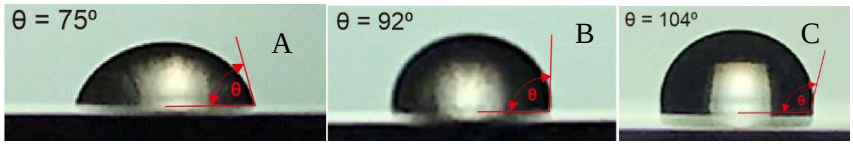

Fig. 5. Visualization of the contact angle on the test specimen

2. Experimental Facilities and Procedures

Figure 6 shows the experimental facilities employed in this study. The test specimens are heated using cartridge heaters, and their temperatures are measured with three K-type thermocouples. An immersion heater maintains the working fluid temperature at the saturation temperature. K-type thermocouples are utilized to measure the temperature of the working fluid. All temperature measurements from the thermocouples are captured and processed using data acquisition systems, specifically the NI cDAQ-9174 and NI 9213, with LabVIEW software. Before the experiments are conducted, all K-type thermocouples are calibrated using LabVIEW. The observation visualizations are captured using a Phantom Miro M310 high-speed camera. The visualizations captured by the high-speed camera are processed using PCC software. The experimental setup also has a lighting system to ensure good visualization results.

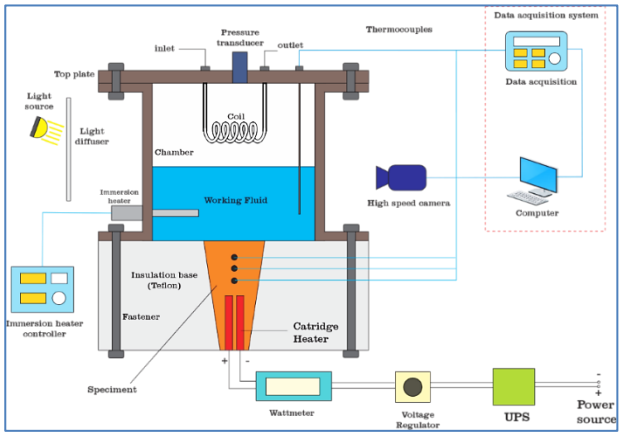

Fig. 6. Experiment facilities

Before the test specimen is mounted on the insulation base, the sides of the specimen are coated with an insulant, Threebond High-Temperature RTV Silicone. This is done to prevent the working fluid from leaking onto the sides of the test specimen, thereby minimizing the heat absorbed by the working fluid other than from the specimen surface.

Deionized water is used as the working fluid. Prior to conducting the experiment, the deionized water is preheated to a temperature close to saturation in order to eliminate any dissolved gases. Throughout the experiment, the temperature of the deionized water is kept at the saturation temperature. The pressure in the chamber is also kept at atmospheric pressure.

The test specimen is heated using a cartridge heater, with power gradually increasing from 5 to 40 watts using a voltage regulator, and monitored using a wattmeter. Temperature data of the test specimen is taken after 5 minutes of adjusting the cartridge heater power to ensure that the specimen's temperature reaches a steady state before recording. There is a copper coil through which water is pumped to condense the working fluid that has undergone a phase change to vapor.

3. Data Processing

The experimental setup exhibits a heat loss of 17% in this study. Heat loss is measured by adjusting the power of the cartridge heater to a specific value and maintaining it for a certain time interval, which increases the temperature of the working fluid. The calculation of heat loss is performed using Eq. (1).

$$\dot{Q}_L = \dot{Q}_{CH} - \frac{m\, c\, (T_1 - T_2)}{t} \quad (1)$$

The calculation of heat transfer from the test specimen to the working fluid is conducted using the one-dimensional Fourier equation, applying the slant equation for the conical cylindrical test specimen as follows:

$$\dot{Q} = -k\, A_{silinder\ conis}\, \frac{dT}{dx} \quad (2)$$

$$\dot{Q} = -k\, \pi\, y^2\, \frac{dT}{dx} \quad (3)$$

$$y = \frac{2}{29}x + 11 \quad (4)$$

$$\dot{q} = \frac{\dot{Q}}{A_{ujung\ silinder\ konis,d=30\ mm}} \quad (5)$$

The surface temperature (T_w) can be calculated by transforming Eq. (3) into Eq. (6), while the BHTC calculation can be done using Eq. (7).

$$\frac{dT}{dx} = -\frac{\dot{Q}}{k\, \pi\, y^2} \quad (6)$$

$$h = \frac{\Delta T}{\dot{q}} \quad (7)$$

where ΔT is the wall superheat temperature, which is obtained from Eq. (8).

$$\Delta T = T_w - T_{sat} \quad (8)$$

In this study, uncertainty analysis was determined by the method of Taylor [34]. From the equations above, it can be determined that the heat flux, $\dot{q}$, is a function of k, T_a, and T_b. Here, T_a and T_b represent the temperatures of the test specimens as depicted by the thermocouples. The uncertainty of the heat flux is expressed in Eq. (9):

$$\frac{\Delta \dot{q}}{|\dot{q}|} = \sqrt{\left(\frac{\partial \dot{q}}{\partial k}.\Delta k\right)^2 + \left(\frac{\partial \dot{q}}{\partial T_a}.\Delta T_a\right)^2 + \left(\frac{\partial \dot{q}}{\partial T_b}.\Delta T_b\right)^2} \quad (9)$$

with the assumption that the thermal conductivity of the test specimen, k, is constant, then

$$\frac{\Delta \dot{q}}{|\dot{q}|} = \sqrt{\left(\frac{\partial \dot{q}}{\partial T_a}.\Delta T_a\right)^2 + \left(\frac{\partial \dot{q}}{\partial T_b}.\Delta T_b\right)^2} \quad (10)$$

From Eq. (10), the average uncertainty of the heat flux, $\dot{q}$, is 0.84%. Using the same method, the average uncertainty of the surface temperature, T_w, is 0.76%, and the average uncertainty of the BHTC, h, is 9.58%.

III. Results and Discussions

1. Effect of Surface Roughness and Nanoceramic Coating

The experimental results regarding the impact of surface modification and nanoceramic coating application are presented in the curves showing the relationship between heat flux and surface temperature of the test specimen, the pool boiling curve, and the relationship

between wall superheat and BHTC, which are displayed in Figure 7-9. Figure 7 shows that the test specimen with the highest surface roughness can maintain a lower surface temperature compared to the test specimens with smoother surfaces at the same heat flux value. Specimen A has the lowest surface temperature, followed by specimens B and C. Test specimens with nanoceramic coating also show an improved ability to maintain surface temperature. Specimens C-1 and C-2 have lower surface temperatures compared to specimen C.

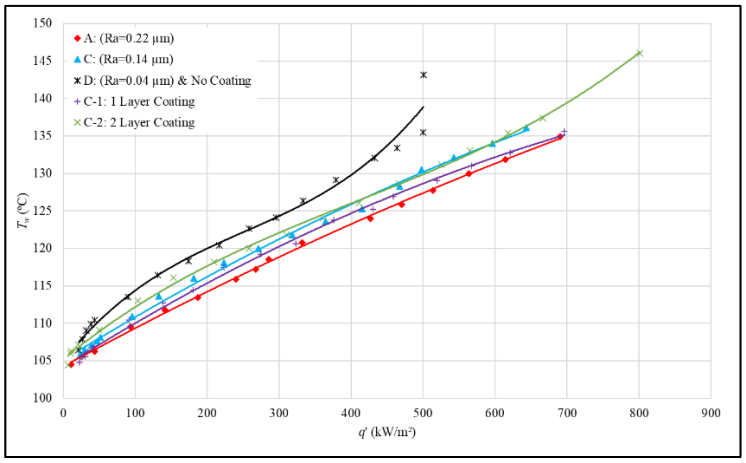

Fig. 7. Graph of the relationship between heat flux and wall temperature

The difference in surface temperature of the test specimens indicates different BHTC, as shown in Figure 8. Test specimens with higher surface roughness have higher BHTC, and vice versa. The results show that specimen A has an average BHTC of 55.69% higher than specimen C, and specimen B has an average BHTC of 31.98% higher than specimen C. The application of nanoceramic coating also affects the BHTC value. In this study, the application of nanoceramic coating increased the BHTC value. Specimen C-1 has an average BHTC of 40.81% higher than specimen C, and specimen C-2 has an average BHTC of 21.42% higher than specimen C.

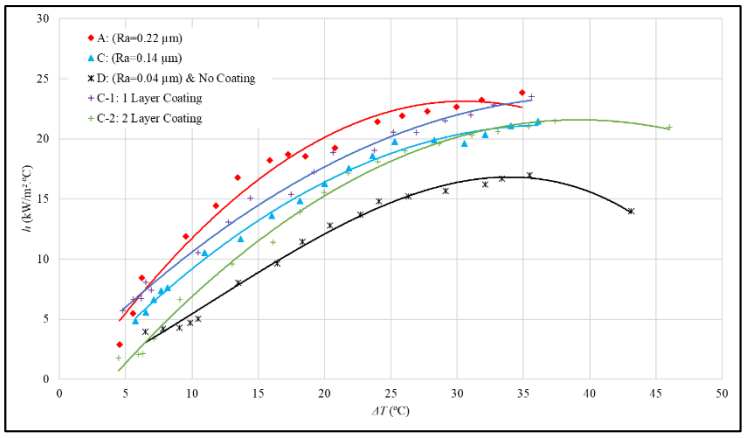

Fig. 8. Boiling heat transfer coefficient

From experiment, it was found that surface roughness affected both the surface temperature and BHTC of the test specimen. The test specimen with more roughness had a lower surface temperature because it can form nucleation sites in the nucleate boiling regime, as is well documented in previous studies [35]-[37]. The scratches on the rough

surface act as nucleation sites for forming vapor bubbles. Nucleation sites are locations where vapor bubbles form on test specimen's surface. In the nucleate boiling regime, vapor bubbles form easily on surfaces with cavities, gaps, or scratches. The more scratches there are on the test specimen's surface, the more available nucleation sites are created. Figure 4 shows the number of scratches on each test specimen. Among the available nucleation sites on the test specimen's surface, those that generate vapor bubbles are referred to as active nucleation sites. The amount of active nucleation sites also affects the frequency of vapor bubble formation. The more active nucleation sites, the higher the frequency of vapor bubble formation, which allows heat to be transferred more effectively from the surface [38].

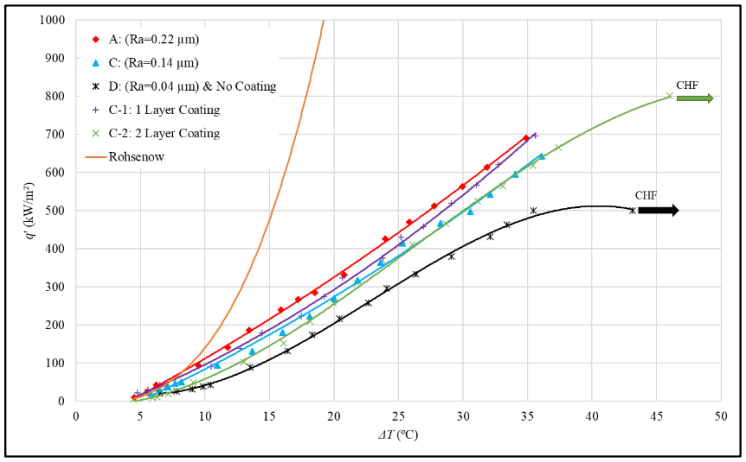

Fig. 9. Pool boiling curve

Fig. 10. Surface visualization: (a) test specimen A at $\dot{q}$ = 21.53 kW/m^2, (b) test specimen B at $\dot{q}$ = 25.61 kW/m^2, and (c) test specimen C at $\dot{q}$ = 27.36 kW/m^2

A comparison of vapor bubble formation on test specimens A, B, and C is shown in Figure 10-11. It can be found that specimens A and B have a higher number of vapor bubbles forming than specimen C. This indicates that the scratches on the rough test specimen affect the formation of vapor bubbles.

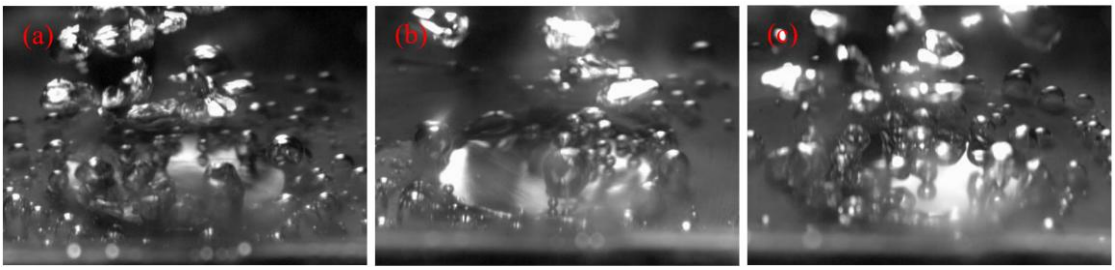

Fig. 11. Surface visualization: (a) test specimen A at $\dot{q}$ = 37.19 kW/m^2, (b) test specimen B at $\dot{q}$ = 39.89 kW/m^2, and (c) test specimen C at $\dot{q}$ = 37.03 kW/m^2

Test specimens whose higher surface roughness was more easily wetted by the working fluid, as shown in Figure 5. The contact angle on test specimens indicates the surface wetting ability. A larger contact angle indicates better wetting ability. Surfaces easily wetted by the fluid optimize the heat transfer process because the fluid that wets the test specimen surface will carry heat away from the surface [39]. The fluid that conveys the thermal energy will then stimulate the forming of bubbles on the test specimen surface.

The application of nanoceramic coating also affected the surface temperature and BHTC. The heat transfer improvement of the test specimen with the coating is due to the presence of nanoceramic particles adhering to the test specimen's surface, which increases the surface area. Additionally, gaps and voids are formed between the coating particles [40]. An illustration of the formation of gaps and voids on the test specimen surface is shown in Figure 12. The formation of voids due to coating on a surface is also explained in the previous study [40],[41].

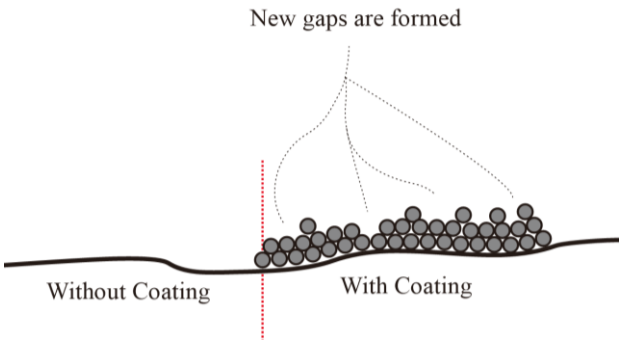

Fig. 12. Illustration of nanoceramic particles on the test specimen surface

The formation of gaps and voids on the test specimen's surface increases the available nucleation sites during the experiment. As the amount of available nucleation sites increases, it can also be expected that the number of active nucleation sites will rise. Therefore, the existence of gaps on the test specimen surface due to the coating particles will enhance the formation of active nucleation sites, resulting to more vapor bubbles forming. The enhanced formation of vapor bubbles will improve the test specimen's heat transfer capability. The increase of heat transfer performance due to coating particle also reported on previous study [42]-[44]. The visualization of vapor bubble formation comparing test specimens with and without coating is given in Figure 13.

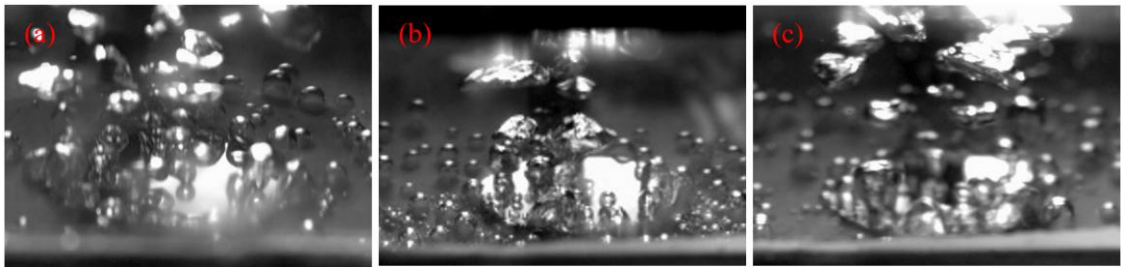

Fig. 13. Surface visualization: (a) test specimen C at $\dot{q}$ = 37.03 kW/m^2, (b) test specimen C-1 at $\dot{q}$ = 37.1 kW/m^2, and (c) test specimen C-2 at $\dot{q}$ = 42.68 kW/m^2

From the pool boiling curve in Figure 9, it can be seen that test specimens C and C-2 experience a notable rise in wall superheat temperature. The elevation in wall superheat temperature is marked by a rightward arrow. For test specimen C, this significant increase

occurs when the heat flux passing through the test specimen exceeds 426.09 kW/m². Meanwhile, for test specimen C-2, the wall superheat temperature significantly increases when the heat flux passing through the specimen exceeds 682.26 kW/m². This phenomenon occured when the test specimen's surface was about to reach the CHF point and enters the transition boiling regime before moving to the film boiling regime. This was indicated by the formation of vapor microlayers on the test specimen's surface and the presence of single bubbles. The significant rise in surface or wall superheat temperature for these two specimens occured when the surface was encased by a vapor layer or microlayer, resulting significant decrease in thermal conductivity. The visualization of the vapor microlayers and single bubbles formation can be seen in Figure 14. From this explanation, it can be concluded that test specimen C will only optimally transfer heat when the heat flux is below 426.09 kW/m², and test specimen C-2 will do so below 682.26 kW/m². Test specimen C-2 has a CHF point 60.12% higher than test specimen C.

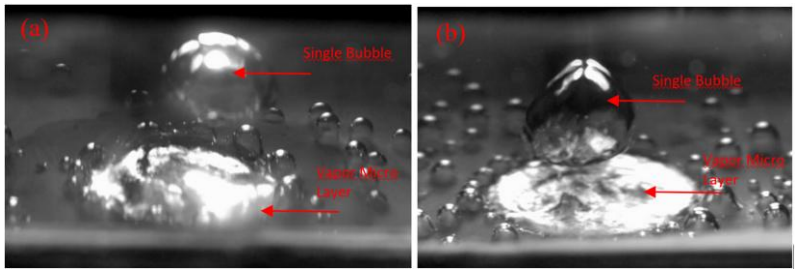

Fig. 14. Visualization of the formation of the vapor microlayer and single bubble on the test specimen (a) C and (b) C-2

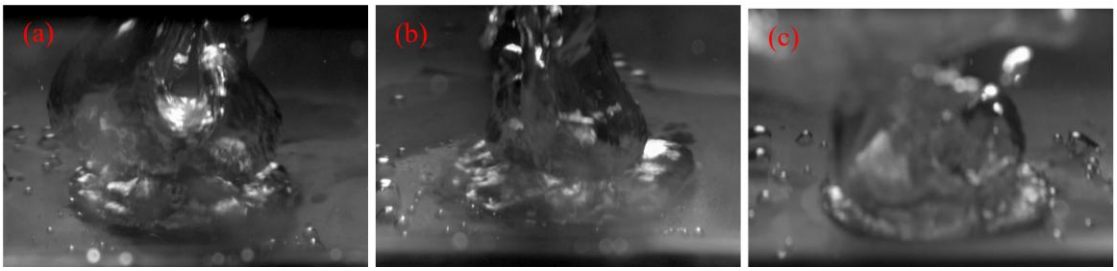

Fig. 15. Visualization of the vapor jet on the test speciment (a) A, (b) B, dan (d) C-1

Due to the power limitations of the cartridge heater, the observation of vapor microlayer and single bubble formation could not be conducted on test specimens A, B, and C-1. Additionally, CHF points for test specimens A, B, and C-1 could not be represented in the pool boiling curve shown in Figure 9. However, continuous columns of vapor, also known as vapor jets, were still present on each test specimen surface. This phenomenon indicates that test specimens A, B, and C-1 conditions remain within the nucleate boiling regime. The visualization of the vapor jet occurring on test specimens A, B, and C-1 shown in Figure 15. The use of another working fluid with a lower saturation temperature would facilitate easier observation of the vapor microlayer and single bubble phenomenon.

Figure 9 compares pool boiling curves for each test specimen against the Rohsenow Equation. From the figure, it can be observed that there are differences between the experimental pool boiling curves and the predicted curves derived from the Rohsenow Equation. These discrepancies arise because the Rohsenow Equation does not account for physical changes on the test specimens's surface, such as variations in surface roughness

and the application of coatings, as employed in this study. Moreover, the heat flux calculations using the Rohsenow Equation exhibit an error margin of ±100% [45].

2. Mechanism of Bubble Formation

The vapor bubbles formation in the pool boiling experiment indicates the shift from the natural convection boiling regime to the nucleate boiling regime. When the test specimen's surface temperature exceeds the working fluid's saturation temperature, small vapor bubbles begin to form on the specimen's surface due to the working fluid undergoes a phase change from liquid to vapor. This bubble formation predominantly occurs in cavities or scratches present on the test specimen's surface, and these areas are referred to as active nucleation sites [46].

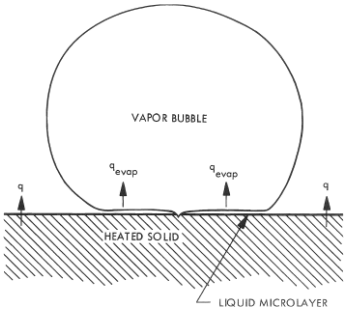

Fig. 16. Illustration of the liquid microlayer [47]

The vapor bubbles that form in the cavities on the test specimen's surface will grow as more of the fluid undergoes phase change [48]. As the vapor bubbles continue to expand, a thin liquid layer develops between the vapor bubble and the test specimen's surface [49]. This layer is known as the liquid microlayer. The appearance of the liquid microlayer can be observed in Figure 16. Rapid evaporation or boiling occurs in the liquid microlayer due to its very low thermal resistance and extremely small thickness [47]. This rapid evaporation process causes the vapor bubbles to grow larger. The liquid microlayer enhance heat transfer coefficient during nucleate pool boiling.

When the bubbles reach a certain size or diameter, they will detach from the test specimen's surface and rise upward. The increasing buoyancy force drives this process as the bubble grows. As soon as the bubble is lifted, the surrounding working fluid will fill the space left, and the bubble formation process will occur again. This process can be observed in Figure 17.

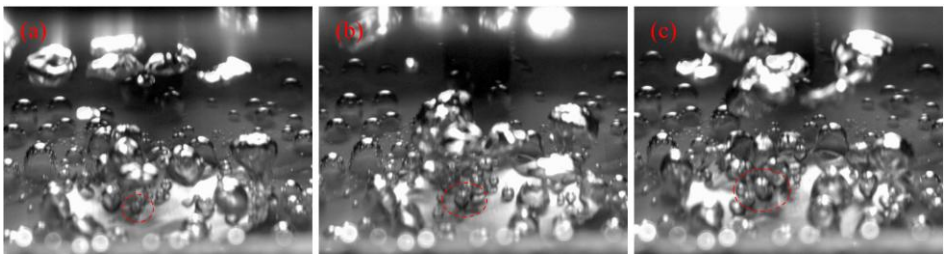

Fig. 17 Visualization of vapor bubbles when (a) small in size, (b) large, and (c) detached due to buoyancy force on test specimen C at $\dot{q}$ = 37.03 kW/m²

When the bubbles are still of a certain size before detaching from the test specimen's surface, it was observed that two or more bubbles merge. This process of merging bubbles

is called bubble coalescence, as shown in Figure 18. The closeness of active nucleation sites leads to bubble coalescence. The existence of bubble coalescence results in vapor bubbles detaching from the test specimen's surface, which is more significant compared to those where bubble coalescence does not occur.

Fig. 18. Visualization of vapor bubbles when (a) before, (b) during, and (c) after bubble coalescence on test specimen B at $\dot{q}$ = 44.02 kW/m²

With an increase in the heat flux, the vapor bubbles formed becomes more numerous and faster along with the rising wall superheat temperature. The increasing amount of bubbles spreading across the test specimen's surface indicates that more available nucleation sites are becoming active nucleation sites. Moreover, the increasing amount of active nucleation sites results in a heightened frequency of bubble coalescence.

As the heat flux increases further, the vapor bubbles, which initially detach from the test specimen's surface as isolated or discrete bubbles, transform into vapor columns and vapor mushrooms, as showed in Figure 15. The formation of vapor columns and vapor mushrooms represents the first transition in nucleate pool boiling [50]. This first transition marks the change in the nucleate pool boiling condition from partial to fully developed nucleate pool boiling. The increase of heat flux and wall superheat temperature during fully developed nucleate boiling causes almost the entire surface to be covered with large vapor mushrooms. Subsequently, dry patches form on the test specimen's surface. These dry patches are areas of the surface that are not covered by the liquid working fluid because blocked by the vapor layer. This condition represents the second transition in nucleate pool boiling [50].

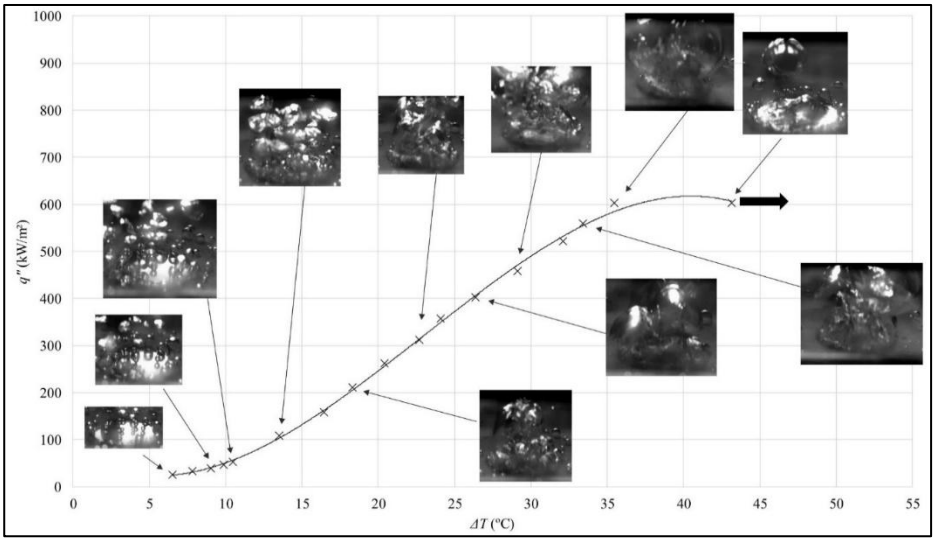

Fig. 19. The formation of vapor bubbles throughout the experiment on test specimen C

As the heat flux continues to increase, the surface eventually becomes fully covered by dry patches, where a vapor layer covers the entire test specimen's surface. At this point, single bubbles also begin to form. This condition signifies that the pool boiling is approaching the CHF. The approach to CHF indicates that the pool boiling regime is transitioning from nucleate boiling to transition boiling. This condition can be observed in Figure 14. From the experiments conducted, the visualization of vapor bubbles on the test specimen's surface, ranging from low to high heat flux, and from the formation of vapor bubbles as discrete bubbles to the formation of vapor mushrooms and single bubbles, can be seen in Figure 19.

IV. Conclusions

In this study, the effect of surface modification, including surface roughness and nanoceramic coating application on a copper conical cylinder, on the pool boiling phenomenon using deionized water as the working fluid was examined in detail. Three test specimens with different surface roughness were used for comparison: 0.22 μm (speciment A), 0.14 μm (speciment B), and 0.04 μm (speciment C). Additionally, three test specimens with different nanoceramic coating applications were compared: specimen C without coating, specimen C-1 with a 1-layer coating, and specimen C-2 with a 2-layer coating. A high-speed camera was used to capture pool boiling visualizations for further analysis.

Based on the discussion above, test specimens with higher surface roughness values have higher BHTC and CHF values. Specimen A has a higher average BHTC 55.69% compared to specimen C, and specimen B has an average BHTC 31.98% higher than specimen C. Specimen C has the lowest CHF compared to specimens A and B, with a value of 426.09 kW/m². Test specimens with higher surface roughness promote more active nucleation sites. The higher amount of active nucleation sites on specimens with greater roughness allows the specimens to maintain surface temperature more effectively, resulting in lower surface temperatures.

Test specimens with nanoceramic coatings show increased BHTC and CHF values. Specimen C-1 has an average BHTC of 40.81% higher than specimen C, and specimen C-2 has an average BHTC of 21.42% higher than specimen C. Specimen C-2 has a CHF value of 60.12% higher than specimen C. The increase in BHTC and CHF for specimens with nanoceramic coating is due to cavities caused by the coating particles, which enhance the active nucleation sites and vapor bubble formation. The increase in active nucleation sites and vapor bubbles facilitate heat removal from the surface, resulting in improved heat transfer performance of the test specimens.

In this study, the power limitations of the cartridge heater prevented the observation of the single bubble and vapor layer phenomenon on test specimens A, B, and C-1. A higher-power cartridge heater or a working fluid with a lower saturation temperature could be implemented in future research to observe single bubble and vapor layer phenomena. Further studies on test specimens with different surface roughness parameters and nanoceramic coatings, as well as observations above the CHF point, are necessary to expand the understanding of boiling heat transfer performance and vapor bubble dynamics on surfaces with varying roughness and nanoceramic coatings.

References

[1] E.J. Choi, J.Y. Park, and M.S. Kim, "A comparison of temperature distribution in PEMFC with single-phase water cooling and two-phase HFE-7100 cooling methods

by numerical study," *International Journal of Hydrogen Energy*, vol. 43, no. 29, pp. 13406–13419, Jul. 2018, doi: 10.1016/j.ijhydene.2018.05.056.

[2] A.K. Sadaghiani, N.S. Saadi, S.S. Parapari, T. Karabacak, M. Keskinoz, and A. Koşar, "Boiling heat transfer performance enhancement using micro and nano structured surfaces for high heat flux electronics cooling systems," *Applied Thermal Engineering*, vol. 127, pp. 484–498, 2017, doi: 10.1016/j.applthermaleng.2017.08.018.

[3] M. Zeng, S. Wang, J. Duan, J. Sun, P. Zhong, and Y. Zhang, "Review of nuclear power development in China: Environment analysis, historical stages, development status, problems and countermeasures," *Renewable and Sustainable Energy Reviews*, vol. 59, pp. 1369–1383, Jun. 2016, doi: 10.1016/j.rser.2016.01.045.

[4] I. Mudawar, "Recent Advances in High-Flux, Two-Phase Thermal Management," *Journal of Thermal Science and Engineering Applications*, vol. 5, no. 2, p. 021012, Jun. 2013, doi: 10.1115/1.4023599.

[5] N. Tran, U. Sajjad, R. Lin, and C.C. Wang, "Effects of surface inclination and type of surface roughness on the nucleate boiling heat transfer performance of HFE-7200 dielectric fluid," *International Journal of Heat and Mass Transfer*, vol. 147, no. xxxx, p. 119015, 2020, doi: 10.1016/j.ijheatmasstransfer.2019.119015.

[6] G. Liang, Y. Chen, J. Wang, Z. Wang, and S. Shen, "Experiments and modeling of boiling heat transfer on hybrid-wettability surfaces," *International Journal of Multiphase Flow*, vol. 144, no. 2, p. 103810, 2021, doi: 10.1016/j.ijmultiphaseflow.2021.103810.

[7] L. Gao, J. Lyu, M. Bai, Y. Li, D. Gao, and L. Shi, "The microchannel combined hydrophobic nanostructure for enhancing boiling heat transfer," *Applied Thermal Engineering*, vol. 194, no. April, p. 116962, 2021, doi: 10.1016/j.applthermaleng.2021.116962.

[8] S. Fan, L. Jiao, K. Wang, and F. Duan, "Pool boiling heat transfer of saturated water on rough surfaces with the effect of roughening techniques," *International Journal of Heat and Mass Transfer*, vol. 159, pp. 1–13, 2020, doi: 10.1016/j.ijheatmasstransfer.2020.120054.

[9] K.K. Wong and K.C. Leong, "Saturated pool boiling enhancement using porous lattice structures produced by Selective Laser Melting," *International Journal of Heat and Mass Transfer*, vol. 121, pp. 46–63, 2018, doi: 10.1016/j.ijheatmasstransfer.2017.12.148.

[10] S. Jun, J. Kim, D. Son, H.Y. Kim, and S.M. You, "Enhancement of Pool Boiling Heat Transfer in Water Using Sintered Copper Microporous Coatings," *Nuclear Engineering and Technology*, vol. 48, no. 4, pp. 932–940, 2016, doi: 10.1016/j.net.2016.02.018.

[11] A. Walunj and A. Sathyabhama, "Comparative study of pool boiling heat transfer from various microchannel geometries," *Applied Thermal Engineering*, vol. 128, pp. 672–683, 2018, doi: 10.1016/j.applthermaleng.2017.08.157.

[12] W. Fogaça, S. Mori, K. Imanishi, K. Okuyama, and J.R.C. Piqueira, "Effect of honeycomb porous plate on critical heat flux in saturated pool boiling of artificial seawater," *International Journal of Heat and Mass Transfer*, vol. 125, pp. 994–1002, 2018, doi: 10.1016/j.ijheatmasstransfer.2018.04.101.

[13] Z. Cao, B. Liu, C. Pregen, Z. Wu, Y. Zhang, X. Wang *et al.*, "Pool boiling heat transfer of FC-72 on pin-fin silicon surfaces with nanoparticle deposition," *International Journal of Heat and Mass Transfer*, vol. 126, pp. 1019–1033, 2018, doi: 10.1016/j.ijheatmasstransfer.2018.05.033.

[14] G. Liang and I. Mudawar, "Review of pool boiling enhancement with additives and nanofluids," *International Journal of Heat and Mass Transfer*, vol. 124, pp. 423–453, 2018, doi: 10.1016/j.ijheatmasstransfer.2018.03.046.
[15] X. Quan, M. Gao, P. Cheng, and J. Li, "An experimental investigation of pool boiling heat transfer on smooth/rib surfaces under an electric field," *International Journal of Heat and Mass Transfer*, vol. 85, pp. 595–608, 2015, doi: 10.1016/j.ijheatmasstransfer.2015.01.083.
[16] A. Abdollahi, M.R. Salimpour, and N. Etesami, "Experimental analysis of magnetic field effect on the pool boiling heat transfer of a ferrofluid," *Applied Thermal Engineering*, vol. 111, pp. 1101–1110, 2017, doi: 10.1016/j.applthermaleng.2016.10.019.
[17] Y. Watanabe, K. Enoki, and T. Okawa, "Nanoparticle layer detachment and its influence on the heat transfer characteristics in saturated pool boiling of nanofluids," *International Journal of Heat and Mass Transfer*, vol. 125, pp. 171–178, 2018, doi: 10.1016/j.ijheatmasstransfer.2018.04.072.
[18] X. Quan, D. Wang, and P. Cheng, "An experimental investigation on wettability effects of nanoparticles in pool boiling of a nanofluid," *International Journal of Heat and Mass Transfer*, vol. 108, pp. 32–40, 2017, doi: 10.1016/j.ijheatmasstransfer.2016.11.098.
[19] Z. Wan, J. Duan, X. Wang, and M. Zheng, "Saturated boiling heat transfer under ultrasound," *International Communications in Heat and Mass Transfer*, vol. 115, p. 104511, 2020, doi: 10.1016/j.icheatmasstransfer.2020.104511.
[20] Y.J. Yang, X.Q. Chen, Y.Y. Huang, and G.Y. Li, "Experimental study on pool boiling of distilled water and HFE7500 fluid under microgravity," *Acta Astronautica*, vol. 143, no. November 2017, pp. 362–371, 2018, doi: 10.1016/j.actaastro.2017.11.011.
[21] T. Halon, B. Zajaczkowski, S. Michaie, R. Rulliere, and J. Bonjour, "Enhanced tunneled surfaces for water pool boiling heat transfer under low pressure," *International Journal of Heat and Mass Transfer*, vol. 116, pp. 93–103, 2018, doi: 10.1016/j.ijheatmasstransfer.2017.09.025.
[22] S. Dahariya and A.R. Betz, "High pressure pool boiling: Mechanisms for heat transfer enhancement and comparison to existing models," *International Journal of Heat and Mass Transfer*, vol. 141, pp. 696–706, Oct. 2019, doi: 10.1016/j.ijheatmasstransfer.2019.07.016.
[23] S. Nukiyama, "The maximum and minimum values of the heat-Q transmitted from metal to boiling water under atmospheric-pressure," *International journal of heat and mass transfer*, vol. 27, no. 7, pp. 959–970, 1934, doi: 10.1016/0017-9310(66)90138-4.
[24] Z. Zhao, X. Ma, S. Li, S. Yang, and L. Huang, "Visualization-based nucleate pool boiling heat transfer enhancement on different sizes of square micropillar array surfaces," *Experimental Thermal and Fluid Science*, vol. 119, no. June, p. 110212, 2020, doi: 10.1016/j.expthermflusci.2020.110212.
[25] Z. Deng, X. Liu, S. Wu, and C. Zhang, "Pool boiling heat transfer enhancement by bi-conductive surfaces," *International Journal of Thermal Sciences*, vol. 167, no. April, p. 107041, 2021, doi: 10.1016/j.ijthermalsci.2021.107041.
[26] T.G. Theofanous, T.N. Dinh, J.P. Tu, and A.T. Dinh, "The boiling crisis phenomenon Part II: dryout dynamics and burnout," *Experimental Thermal and Fluid Science*, vol 26, pp. 793-810, 2002, doi: 10.1016/S0894-1777(02)00193-0.

[27] A. Sur, Y. Lu, C. Pascente, P. Ruchhoeft, and D. Liu, "Pool boiling heat transfer enhancement with electrowetting," *International Journal of Heat and Mass Transfer*, vol. 120, pp. 202–217, 2018, doi: 10.1016/j.ijheatmasstransfer.2017.12.029.
[28] U. Sajjad, A. Sadeghianjahromi, H. M. Ali, and C. C. Wang, "Enhanced pool boiling of dielectric and highly wetting liquids – A review on surface engineering," *Applied Thermal Engineering*, vol. 195, no. January, p. 117074, 2021, doi: 10.1016/j.applthermaleng.2021.117074.
[29] H. Seo, Y. Lim, H. Shin, and I.C. Bang, "Effects of hole patterns on surface temperature distributions in pool boiling," *International Journal of Heat and Mass Transfer*, vol. 120, pp. 587–596, 2018, doi: 10.1016/j.ijheatmasstransfer.2017.12.066.
[30] J. Zhou, P. Xu, B. Qi, Y. Zhang, and J. Wei, "Effects of micro-pin-fins on the bubble growth and movement of nucleate pool boiling on vertical surfaces," *International Journal of Thermal Sciences*, vol. 171, no. June 2021, p. 107186, 2022, doi: 10.1016/j.ijthermalsci.2021.107186.
[31] M.M. Petrovic and V.D. Stevanovic, "Pool boiling simulation with two-fluid and grid resolved wall boiling model," *International Journal of Multiphase Flow*, vol. 144, no. April, p. 103806, 2021, doi: 10.1016/j.ijmultiphaseflow.2021.103806.
[32] J. Yuan, X. Ye, and Y. Shan, "Modeling of the bubble dynamics and heat flux variations during lateral coalescence of bubbles in nucleate pool boiling," *International Journal of Multiphase Flow*, vol. 142, p. 103701, 2021, doi: 10.1016/j.ijmultiphaseflow.2021.103701.
[33] S. Xie, M.S. Beni, J. Cai, and J. Zhao, "Review of critical-heat-flux enhancement methods," *International Journal of Heat and Mass Transfer*, vol. 122, pp. 275–289, 2018, doi: 10.1016/j.ijheatmasstransfer.2018.01.116.
[34] J.R. Taylor, *An introduction to error analysis: the study of uncertainties in physical measurements*, 2. ed. Sausalito, Calif: University Science Books, 1997.
[35] J.S. Kim, A. Girard, S. Jun, J. Lee, and S.M. You, "Effect of surface roughness on pool boiling heat transfer of water on hydrophobic surfaces," *International Journal of Heat and Mass Transfer*, vol. 118, pp. 802–811, 2018, doi: 10.1016/j.ijheatmasstransfer.2017.10.124.
[36] N. Tran, U. Sajjad, R. Lin, and C.C. Wang, "Effects of surface inclination and type of surface roughness on the nucleate boiling heat transfer performance of HFE-7200 dielectric fluid," *International Journal of Heat and Mass Transfer*, vol. 147, no. xxxx, Art. no. xxxx, 2020, doi: 10.1016/j.ijheatmasstransfer.2019.119015.
[37] B.D. Bock, J.P. Meyer, and J.R. Thome, "Falling film boiling and pool boiling on plain circular tubes : Influence of surface roughness , surface material and saturation temperature on heat transfer and dryout," *Experimental Thermal and Fluid Science*, vol. 109, no. July, Art. no. July, 2019, doi: 10.1016/j.expthermflusci.2019.109870.
[38] M.R. Mata Arenales, S.K. Sujith, L.S. Kuo, and P.H. Chen, "Surface roughness variation effects on copper tubes in pool boiling of water," *International Journal of Heat and Mass Transfer*, vol. 151, p. 119399, 2020, doi: 10.1016/j.ijheatmasstransfer.2020.119399.
[39] P. Bai, L. Zhou, X. Huang, and X. Du, "How wettability affects boiling heat transfer: A three-dimensional analysis with surface potential energy," *International Journal of Heat and Mass Transfer*, vol. 175, p. 121391, 2021, doi: 10.1016/j.ijheatmasstransfer.2021.121391.
[40] I.S. Kiyomura, L.L. Manetti, A.P. da Cunha, G. Ribatski, and E.M. Cardoso, "An analysis of the effects of nanoparticles deposition on characteristics of the heating

surface and ON pool boiling of water," *International Journal of Heat and Mass Transfer*, vol. 106, pp. 666–674, 2017, doi: 10.1016/j.ijheatmasstransfer.2016.09.051.
[41] W. Li, R. Dai, M. Zeng, and Q. Wang, "Review of two types of surface modification on pool boiling enhancement: Passive and active," *Renewable and Sustainable Energy Reviews*, vol. 130, no. June, Art. no. June, 2020, doi: 10.1016/j.rser.2020.109926.
[42] H. Moghadasi and H. Saffari, "Experimental study of nucleate pool boiling heat transfer improvement utilizing micro/nanoparticles porous coating on copper surfaces," *International Journal of Mechanical Sciences*, vol. 196, no. January, Art. no. January, 2021, doi: 10.1016/j.ijmecsci.2021.106270.
[43] Z. Cao, Z. Wu, A.D. Pham, Y. Yang, S. Abbooc, P. Falkman *et al.*, "Pool boiling of HFE-7200 on nanoparticle-coating surfaces: Experiments and heat transfer analysis," *International Journal of Heat and Mass Transfer*, vol. 133, pp. 548–560, 2019, doi: 10.1016/j.ijheatmasstransfer.2018.12.140.
[44] L. Mao, W. Zhou, X. Hu, Y. He, G. Zhang, L. Zhang *et al.*, "Pool boiling performance and bubble dynamics on graphene oxide nanocoating surface," *International Journal of Thermal Sciences*, vol. 147, no. January 2019, Art. no. January 2019, 2020, doi: 10.1016/j.ijthermalsci.2019.106154.
[45] Y.A. Cengel, *Heat Transfer: A Practical Approcah*. Mc Graw-Hill, 2003.
[46] M. M. Mahmoud and T. G. Karayiannis, "Pool boiling review: Part I – Fundamentals of boiling and relation to surface design," *Thermal Science and Engineering Progress*, vol. 25, no. May, Art. no. May, 2021, doi: 10.1016/j.tsep.2021.101024.
[47] L.S. Tong and Y.S. Tang, *Boiling Heat Transfer And Two-Phase Flow*. 1997. [Online]. Available: http://books.google.com/books?id=_4PeDDusJykC
[48] U. Sajjad, A. Sadeghianjahromi, H. M. Ali, and C. C. Wang, "Enhanced pool boiling of dielectric and highly wetting liquids - a review on enhancement mechanisms," *International Communications in Heat and Mass Transfer*, vol. 119, p. 104950, 2020, doi: 10.1016/j.icheatmasstransfer.2020.104950.
[49] J. Kim, "Review of nucleate pool boiling bubble heat transfer mechanisms," *International Journal of Multiphase Flow*, vol. 35, no. 12, Art. no. 12, 2009, doi: 10.1016/j.ijmultiphaseflow.2009.07.008.
[50] S.G. Kandlikar, *Handbook of Phase Change: Boiling and Condensation*. Taylor & Francis, 1999.